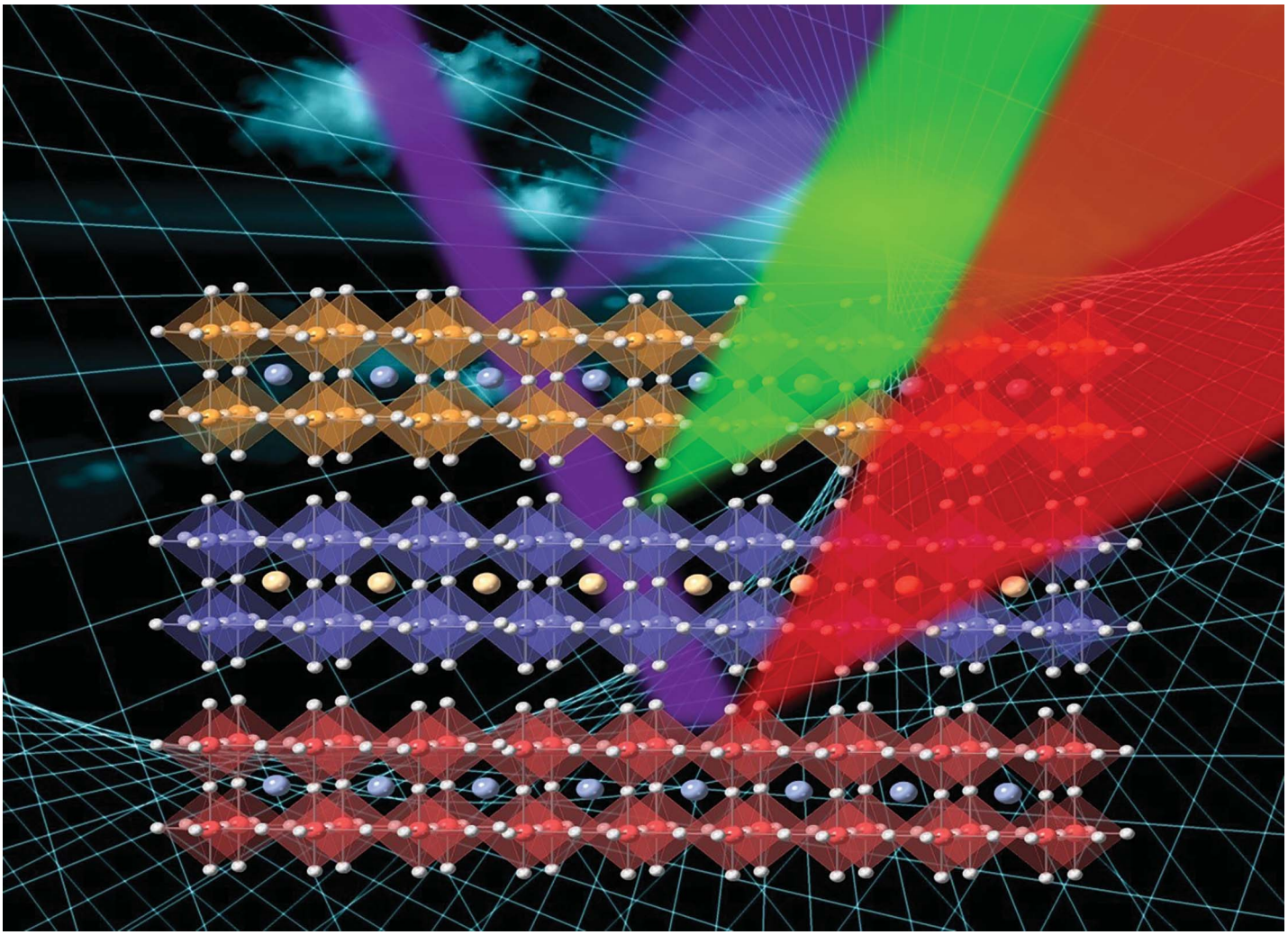

Showcasing research from the laboratories of Professors Jianbo Gao, Hugo Sanabria and Apparao Rao, Department of Physics and Astronomy, Clemson University, Clemson, SC 29634, USA.

The correlation between phase transition and photoluminescence properties of $CsPbX_3$ (X = Cl, Br, I) perovskite nanocrystals

Perovskite nanocrystals (NCs) have aroused tremendous interests in optoelectronic applications due to their high quantum yield and carrier mobility. In this work, the correlation between the structural phase transition and emissive properties of all-inorganic perovskite $CsPbX_3$ (X = Cl, Br, and I) NCs was investigated using steady-state photoluminescence (PL) and time resolved PL spectroscopies. A correlation between the electronic structure and exciton dynamics with the structural phase transition of $CsPbX_3$ was uncovered. This work provides a deeper insight into the role of phase-transition on the photo-physics of perovskite materials.

As featured in:

See Apparao M. Rao, Jianbo Gao *et al.*, *Nanoscale Adv.*, 2020, **2**, 4390.

ROYAL SOCIETY OF CHEMISTRY

rsc.li/nanoscale-advances

Registered charity number: 207890

Nanoscale Advances

ROYAL SOCIETY OF CHEMISTRY

COMMUNICATION

View Article Online
View Journal | View Issue

Cite this: *Nanoscale Adv.*, 2020, **2**, 4390

Received 30th June 2020
Accepted 5th July 2020

DOI: 10.1039/d0na00545b

rsc.li/nanoscale-advances

The correlation between phase transition and photoluminescence properties of $CsPbX_3$ (X = Cl, Br, I) perovskite nanocrystals†

Jun Yi,[ab] Xueying Ge,[a] Exian Liu,[ab] Tong Cai,[c] Chujun Zhao,[b] Shuangchun Wen,[b] Hugo Sanabria,[a] Ou Chen,[c] Apparao M. Rao *[a] and Jianbo Gao*[a]

We report a correlation between the structural phase transition of $CsPbX_3$ (X = Cl, Br, I) nanocrystals (NCs) and their temperature-dependent steady-state photoluminescence (PL) and time-resolved PL (TRPL). In contrast to $CsPbBr_3$ and $CsPbI_3$ NCs which exhibited a continuous blue-shift in their band gap with increasing temperature, the $CsPbCl_3$ exhibited a blue shift until ~193 K, followed by a red shift until room temperature. We attribute this change from a blue to a red shift to a structural phase transition in $CsPbCl_3$, which also manifested in the temperature dependent TRPL. This pronounced phase transition in $CsPbCl_3$ NCs is probably due to the condensation of its vibrational modes at low temperature, and the presence of the weak quantum confinement effect. Notably, the exciton recombination lifetimes showed a similar reverse trend due to the phase transition in $CsPbCl_3$, which has not been reported previously.

A phase transition is one of the most fundamental physical phenomena in solid-state physics as it could also influence the electrical, optical, magnetic, mechanical, and chemical properties of the materials. It is particularly important for emerging perovskite semiconductors, which have attracted much attention due to their superior electronic and optical properties. Bulk perovskite semiconductors are used in myriad applications such as light-emitted diodes (LED),[1] photovoltaics,[2–4] X-ray detectors, lasers, and other optoelectronic devices[5,6] because of their highly mobile free charge carriers,[7–9] high absorption coefficients,[10,11] low exciton binding energies,[12,13] and long charge-carrier diffusion lengths.[14] Not surprisingly, the perovskite nanocrystals (NCs) are also attracting much attention because of their unique tunable optical properties, which stem from their size, structure, shape, and tunable compositions.[15–17] Notably, perovskite NCs offer more stable phases, which are not achievable in the bulk materials. For instance, cubic phase α-$CsPbI_3$ NC-based solar cells exhibit more than 15% power conversion efficiency under ambient conditions and are stable for more than 100 hours, while the bulk $CsPbI_3$ is an unstable semiconductor under ambient conditions.[18] Traditionally, phase transitions are widely characterized using X-ray diffraction (XRD) to provide detailed information of the lattice structure, which in turn could depend on temperature, pressure, light, electric field, *etc.* For instance, in bulk and nanocrystalline perovskite materials, temperature-dependent XRD has been used to investigate the phase transitions;[19,20] however, there are only a few reports that correlate the phase transition with optical properties, which is of important for their applications in optoelectronics.

In this report, we investigate the temperature-dependent PL of all-inorganic perovskite $CsPbX_3$ (X = Cl, Br, and I) NCs using steady-state PL and time-resolved PL (TRPL) spectroscopies to correlate their phase transition with their emission properties. We found that the band gap energies and lifetimes increase continuously with the temperature in $CsPbBr_3$ and $CsPbI_3$ NCs; however, $CsPbCl_3$ NCs exhibited a blue shift until their phase transition temperature of ~193 K, followed by a red-shift until room temperature. Also, the lifetimes of $CsPbCl_3$ NCs decreased up to their phase transition temperature, above which they showed an increasing trend.

All-inorganic perovskite $CsPbX_3$ NCs were synthesized using a hot-injection method (see Experimental section).[21] The cubic lattice framework of $CsPbX_3$ consists of the corner-sharing PbX_6 octahedra with Cs^+ embedded in the interstitial voids (Fig. 1a). The room temperature PL and absorption spectra of $CsPbX_3$ NC dispersions in hexane are shown in Fig. 1b, and the energy difference between the excitonic absorption peak and PL peak (or Stokes shift, which stems from the exciton relaxation processes) is evident.[22] From detailed transmission

[a]*Department of Physics and Astronomy, Clemson Nanomaterials Institute, Clemson University, Clemson, SC 29634, USA. E-mail: arao@clemson.edu; jianbogao.nano@gmail.com*

[b]*Key Laboratory for Micro/Nano Optoelectronic Devices of Ministry of Education, Hunan Provincial Key Laboratory of Low-Dimensional Structural Physics and Devices, School of Physics and Electronics, Hunan University, Changsha 410082, China*

[c]*Department of Chemistry, Brown University, Providence, RI 02912, USA*

† Electronic supplementary information (ESI) available. See DOI: 10.1039/d0na00545b

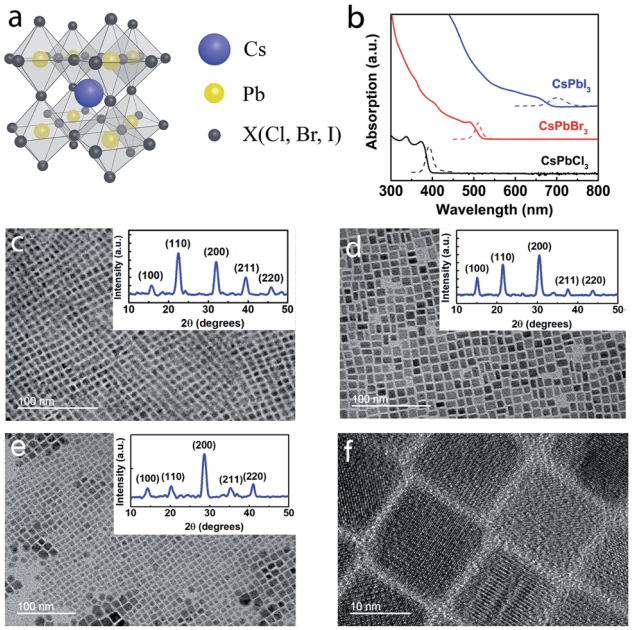

Fig. 1 Structural characterization of $CsPbX_3$ nanocrystals (NCs). (a) A schematic crystal structure of a cubic $CsPbX_3$ perovskite. (b) Room temperature absorption (solid) and PL spectra (dashed) of $CsPbX_3$ NCs in a hexane solution. TEM images of (c) $CsPbCl_3$, (d) $CsPbBr_3$, and (e) $CsPbI_3$ NCs. (f) High-resolution TEM image of $CsPbI_3$ NCs. The insets in panels (c–e) are the corresponding room temperature XRD patterns.

electron microscopy (TEM) analyses, the average NC size was found to be ~7.2, ~9.1, and ~14.9 nm for $CsPbCl_3$, $CsPbBr_3$, and $CsPbI_3$, respectively (Fig. 1c–e). Fig. 1f shows the high-resolution TEM image of $CsPbI_3$ NCs. The Bohr radii of $CsPbCl_3$, $CsPbBr_3$, and $CsPbI_3$ are known to be ~5, ~7, and ~12 nm,[23] respectively, and the NCs exhibit weak quantum confinement since the ratio of NC size to the respective Bohr radius is ~1.24 to ~1.44. It is well-known that organo-lead halide perovskites have three phases which include the high temperature cubic phase (>315 K), room temperature tetragonal phase (160–330 K) and low temperature orthorhombic phase (<160 K). The room temperature XRD patterns of the $CsPbX_3$ (X = Cl, Br, I) NCs used in this study are shown as insets in Fig. 1c–e. The $CsPbI_3$ NCs exhibit the cubic phase[24] with peaks at $2\theta = 14.2$, 20.2, 28.6, 35.3, and 41.0° corresponding to diffractions from the (100), (110), (200), (211) and (220) planes, and a shift in the diffraction peaks towards a higher angle (2θ) as X changes from I to Cl is ascribed to the lattice contraction caused by the shrinking size of the halide ion from I^- to Cl^-.[23] The XRD data confirmed the formation of $CsPbX_3$ quantum dots with the space group $Pm\bar{3}m$.[25]

For the temperature-dependent studies, thin film samples of $CsPbX_3$ NCs were prepared by drop-casting the respective dispersions on quartz slides, and their temperature-dependent PL data were acquired (Fig. 2a–c). The excitation energies (wavelengths) used in this study for $CsPbCl_3$, $CsPbBr_3$, and $CsPbI_3$ NCs were 4.13 eV (300 nm), 3.54 eV (350 nm), and 2.48 eV (500 nm), respectively. It is evident that the PL intensity decreases in all three panels (a–c) with increasing temperature, which is due to the presence of increased non-radiative processes at high temperature. Furthermore, the PL emission peaks of $CsPbBr_3$ and $CsPbI_3$ NCs exhibit a blue shift with increasing temperature, which is in contrast to the temperature-dependent shift in the PL emission peak of $CsPbCl_3$ NCs (dashed arrows in Fig. 1a–c). As expected, a thermal broadening of the full-width-at-half-maximum (FWHM) intensity is also observed with increasing temperature in Fig. 2d–f. Using

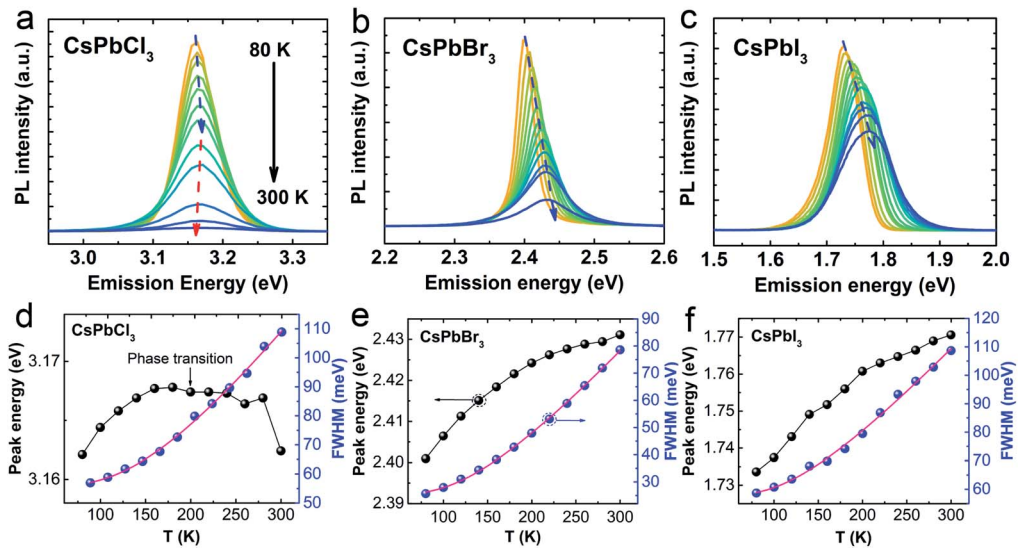

Fig. 2 Steady-state PL characteristics of $CsPbX_3$ NCs. Steady-state PL spectra of (a) $CsPbCl_3$, (b) $CsPbBr_3$, and (c) $CsPbI_3$ NCs in the temperature range of 80 K–300 K. Temperature-dependent full-width-at-half-maximum (FWHM) intensities and the emission peak energies of (d) $CsPbCl_3$, (e) $CsPbBr_3$, and (f) $CsPbI_3$ NCs. Blue and red dashed arrows in (a–c) show the blue and red shift of emission peak energy with the increasing temperature. The red traces in (d–f) represent least square fits to the temperature dependent FWHM data and the black traces serve as a guide to the eye.

different excitation energies, examples of low temperature 2D PL contour maps of $CsPbBr_3$ NCs are shown in Fig. S1 (see the ESI†) to demonstrate that the shift is independent of excitation energy.

The temperature-dependent band gap of perovskites reveals an unusual trend compared to traditional semiconductors. The band gaps of $CsPbBr_3$ and $CsPbI_3$ exhibited a blue shift with increasing temperature, which is in contrast to that predicted by the Varshni's empirical model in which electron–phonon coupling usually dominates and leads to a red shift of the band gap with increasing temperature.[26] A blue shift in the band gap energy can arise from an interplay of contributions from the lattice thermal expansion and electron–phonon coupling.[27,28] The lattice thermal expansion has been reported to dominate and decrease the interaction between the orbitals in the valence band maximum (s orbital of Cs and p orbital of X), which leads to a decrease in the valence bandwidth and an increase in the band gap.[27,29] Similar to $CsPbBr_3$ and $CsPbI_3$, the band gap of $CsPbCl_3$ exhibited a blue shift in the 80–180 K temperature range. However, it showed a red shift in the temperature range from 200–300 K, which implies that the electron-phonon coupling dominates in $CsPbCl_3$ at higher temperatures. This change from a blue to a red shift is attributed to the low temperature phase transition ~193 K in $CsPbCl_3$ which is unique to $CsPbCl_3$, and absent in $CsPbBr_3$ and $CsPbI_3$. At ~193 K, $CsPbCl_3$ deviated from its centrosymmetric structure, which was confirmed by electron paramagnetic resonance, X-ray diffraction, photoacoustic and Raman spectroscopies.[30–33] The low-temperature Raman spectroscopy of $CsPbCl_3$ revealed a unique change in the behavior of its vibration modes. The Raman modes located at 76 cm^{-1}, 95 cm^{-1}, 123 cm^{-1} and <50 cm^{-1} start to disappear as the temperature increases above 193 K, which has been referred to as the condensation of these vibration modes in $CsPbCl_3$ at 193 K.[34] When the temperature decreases below 193 K, the structural phase of $CsPbCl_3$ changes from orthorhombic to monoclinic,[30] which was reported in $CsPbCl_3$ bulk materials.[30–34] However, this phase transition is not exhibited by $CsPbCl_3$ quantum dots because of the strong quantum confinement condition,[35] but is exhibited by $CsPbCl_3$ NCs used in this study due to their weak quantum confinement condition.

To gain a deeper understanding of the mechanism, the temperature-dependent band gap and spectral broadening of PL for $CsPbX_3$ NCs are shown in Fig. 2d–f. The broadening with temperature is mainly due to the electron–phonon coupling which includes electron–acoustic phonon and electron–longitudinal optical (LO) phonon coupling.[29] In most semiconductors, the electron–LO phonon interaction dominates at temperatures above 80 K, thus neglecting the electron–acoustic phonon coupling; the broadening of PL linewidth can be express as[36]

$$\Gamma(T) = \Gamma_0 + \gamma_{LO} \Big/ \left(e^{\frac{E_{LO}}{k_B T}} - 1 \right) \quad (1)$$

where, Γ_0 represents the inhomogeneously broadened linewidth due to scattering by disorder and imperfections in the NCs. The second term represents homogeneous broadening which results from scattering of LO phonons (Fröhlich interaction) with an energy E_{LO} and electron–phonon coupling strength of γ_{LO}, and k_B is the Boltzmann constant. The least-square fits to the linewidth of emission peaks are shown as the red traces in Fig. 2d–f, and the extracted parameters are listed in Table 1. In particular, the E_{LO} value increases from 33.8 meV for heavy iodine anions to 38.0 meV for lighter chloride anions. Furthermore, the γ_{LO} is highest in $CsPbCl_3$, followed by that of $CsPbBr_3$ and $CsPbI_3$, which is due to the lower high-frequency values of the dielectric function of $CsPbCl_3$ and $CsPbBr_3$.[37] For $CsPbX_3$, the displacement of Pb atoms dominates the acoustic mode vibrations, while the displacement of halogen anions dominates optical mode vibrations.[38] Thus, the E_{LO} of the $CsPbX_3$ scales with the halogen anion mass, namely, the lighter halogen anions exhibit higher vibration frequency resulting in a higher E_{LO}. In addition, by fitting the temperature-dependent PL intensity using the Arrhenius equation,[29,35] the binding energies of $CsPbCl_3$, $CsPbBr_3$, and $CsPbI_3$ NCs were obtained as 133.19 meV, 52.98 meV, and 60.18 meV, which are close to the values reported in previous studies.[23,35] The difference is mainly due to the quantum confinement effect resulting from the different sizes of nanocrystals.

Table 1 Extracted linewidth parameters of $CsPbX_3$ NCs

Sample	Γ_0 (meV)	γ_{LO} (meV)	E_{LO} (meV)
$CsPbCl_3$	56.5 ± 0.82	176.2 ± 22.75	38.0 ± 2.69
$CsPbBr_3$	25.4 ± 0.38	160.4 ± 9.27	36.1 ± 1.18
$CsPbI_3$	57.8 ± 1.11	139.1 ± 23.18	33.8 ± 3.33

As mentioned, we attribute the unusual red shift with decreasing temperature and a common blue shift with increasing temperature to the phase transition in $CsPbCl_3$ NCs. This is also consistent with the temperature-dependent TRPL results as shown in Fig. 3, which can be manifested by the exciton decay dynamics. In general, TRPL data is analyzed in terms of single ($I = I_0 + A_1 \exp(-t/t_1)$) or bi-exponential ($I = I_0 + A_1 \exp(-t/t_1) + A_2 \exp(-t/t_2)$) decay processes, where I_0 represents the offset of normalized PL intensity, and (A_1, t_1) and, (A_2, t_2) are the relative weights and lifetimes, respectively. In the case of $CsPbCl_3$, it exhibited a unique trend: in the 80–180 K (200–300 K) range, its lifetimes decrease (increase) with increasing temperature, and the phase transition temperature of 180 K is consistent with that induced from the steady-state PL. In contrast, in the case of $CsPbBr_3$ (single exponential process) and $CsPbI_3$ (bi-exponential process, see Table S1 in ESI†), their lifetimes increase with increasing temperature, which is consistent with the recently reported trends due to exciton fission.[35] Its increasing trend in the 200–300 K range was similar to that of $CsPbBr_3$ and $CsPbI_3$. From 180 to 300 K, the structural phase of $CsPbCl_3$ is orthorhombic, which is the same as the structural phase of $CsPbBr_3$ and $CsPbI_3$, hence the lifetime of $CsPbCl_3$ shows the same increasing trend as the lifetime of $CsPbBr_3$ and $CsPbI_3$. However, for temperatures below 193 K, the structural phase of $CsPbCl_3$ changes from orthorhombic to monoclinic, leading to a reverse trend in the temperature-dependent lifetime. This novel finding clearly suggests that the

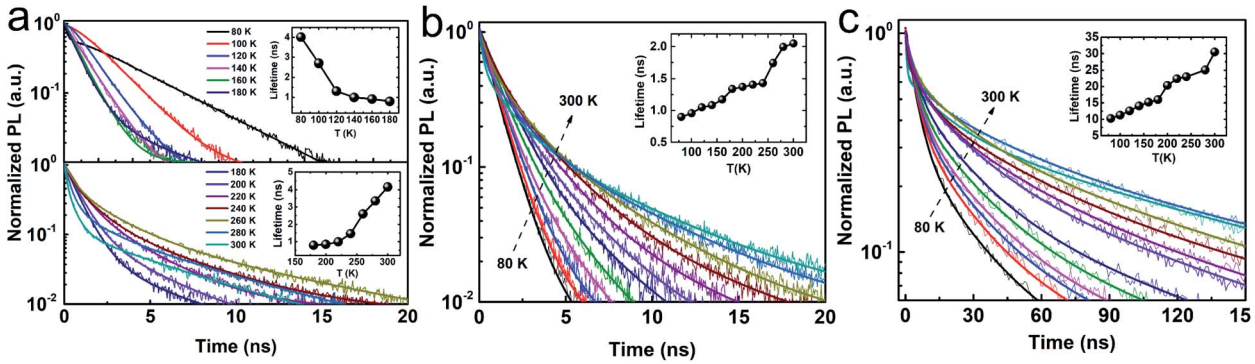

Fig. 3 TRPL characteristics of $CsPbX_3$ NCs. Normalized TRPL data of (a) $CsPbCl_3$, (b) $CsPbBr_3$, and (c) $CsPbI_3$ NCs in the temperature range from 80–300 K. Each colored trace in the figure represents TRPL data that were collected at a specific temperature (legends shown in panel (a)). The solid traces are fits to the data, and the insets show the corresponding lifetimes. For clarity, two sub-panels are shown in panel (a).

excitonic recombination lifetime is intimately coupled with the structural phase transition. Such phase transition induced trend reversal in the temperature-dependent band gap and lifetimes reveals the correlation between phase transition, electronic structure, and exciton dynamics, which can provide significant guidance for phase transition-related electronic and optical properties of the perovskite.

Conclusions

In summary, we investigated the temperature-dependent PL and TRPL of $CsPbX_3$ NCs in the 80 to 300 K temperature range, which revealed a correlation between phase transition, electronic structure, and exciton dynamics. In particular, the low temperature phase transition of $CsPbCl_3$ at ~193 K resulted in a reverse temperature dependence of band gap that red-shifted with increasing temperature until 300 K. Furthermore, the exciton recombination lifetimes showed the similar reverse trend due to the phase transition, which has not been reported previously. Overall, this study presents comprehensive temperature-dependent spectroscopic signatures of all-inorganic perovskites $CsPbX_3$ NCs, which provide a deeper insight into the effect of phase-transition on the low temperature photo-physics of perovskite materials.

Experimental

Synthesis and characterization

Chemicals. Cesium carbonate (Cs_2CO_3, 99.9%), lead(II) acetate trihydrate ($Pb(OAc)_2 \cdot 3H_2O$, 99.999%), benzoyl chloride (99%), benzoyl bromide (97%), iodotrimethylsilane (97%), oleic acid (OA, technical grade, 90%), oleylamine (OAm, technical grade, 70%), and 1-octadecene (ODE, technical grade, 90%) were purchased from Sigma-Aldrich. Toluene, hexanes, and ethyl acetate were purchased from Fisher Scientific. All chemicals were used as received without further purification.

Synthesis of $CsPbX_3$ (X = Cl, Br, and I) perovskite nanocrystals (NCs). $CsPbX_3$ (X = Cl, Br, I) NCs were synthesized using the hot-injection method following a modified process published in the literature.[26] In a typical synthesis, Cs_2CO_3 (32 mg, 0.2 mmol) and $Pb(OAc)_2 \cdot 3H_2O$ (137 mg, 0.36 mmol) were mixed with OA (0.6 mL), OAm (2.0 mL) and ODE (10.0 mL) and then added to a 50 mL three-neck flask. The mixture was first degassed for 5 min at room temperature, and then for 1 hour when the temperature was increased to 120 °C. The mixture became transparent after all precursors dissolved well and then the flask was heated to 200 °C in a N_2 atmosphere (170 °C for $CsPbBr_3$, and 165 °C for $CsPbI_3$). Upon reaching this temperature, 0.40 mL benzoyl chloride (0.30 mL benzoyl bromide for $CsPbBr_3$, and 0.30 mL iodotrimethylsilane for $CsPbI_3$) was injected into the solution which immediately became turbid. After 10 s, the solution was cooled down to room temperature using an ice bath which resulted in a stable dispersion.

Purification. 15 mL of ethyl acetate was added to the above described dispersions and the mixtures were centrifuged for 10 min at 7000 rpm. The supernatant was discarded and the precipitate was dispersed in 10 mL toluene (or hexane). The dispersion was again centrifuged for 5 min at 4500 rpm to separate nanocrystals of larger sizes. The clear supernatant solution was kept for further characterization.

Characterization. UV-Vis absorption spectra were measured using an Agilent Technologies Cary 5000 UV-Vis spectrophotometer. $CsPbX_3$ (X = Cl, Br, and I) perovskite nanocrystals were dissolved in toluene for the measurements. TEM measurements were performed on a JEOL 2100F operated at 200 kV. $CsPbX_3$ (X = Cl, Br, and I) perovskite nanocrystals were diluted in toluene, then drop cast on a 300-mesh copper TEM grid and dried under ambient conditions. X-ray diffraction (XRD) patterns were obtained on a Bruker D8 Discovery 2D X-ray Diffractometer equipped with a Vantec 500 2D area detector operating with Cu Kα (λ = 1.541 Å) radiation. The NC samples were drop-cast on the glass slides and evaporated under mild heating.

Temperature dependent steady-state PL and TRPL spectra

The temperature dependent PL experiments were performed using a modular spectrofluorometer system (HORIBA Nanolog) which consisted of a Xenon lamp (HORIBA FL-1039), an excitation monochromator, a sample-compartment module, an emission spectrometer and a CCD detector (HORIBA Symphony II). The TRPL spectra were measured by using

a spectrofluorometer (HORIBA FluoroLog FL3-22) equipped with a picosecond photon detection module (TBX-05) and a 375 nm laser source (NanoLED N-375L) controlled by using a single photon counting controller (FluoroHub). The dispersions of $CsPbX_3$ QDs were drop-casted onto quartz substrates and then placed inside an optical cryostat (JANIS, ST-100 equipped with a Turbolab 350) which was illuminated by using the Xenon lamp and laser. The temperature of the cryostat was controlled by using a temperature controller (Lake Shore, Model 325).

Conflicts of interest

The authors declare no conflict of interest.

Acknowledgements

The support provided by the China Scholarship Council (CSC) during a visit of Jun Yi to Clemson is acknowledged. We also wish to thank Russell Reynolds, Barrett Barker, and Michael Denz at Clemson University for their instrumental and technical support. A. M. Rao acknowledges financial support for this project through the R. A. Bowen Professorship at Clemson University.

Notes and references

1 M. L. Lai, F. Deschler, H. J. Snaith, T. Bein, D. Credgington, Z.-K. Tan, F. Hanusch, A. Sadhanala, R. S. Moghaddam, R. Higler, M. Price, P. Docampo, R. H. Friend and L. M. Pazos, *Nat. Nanotechnol.*, 2014, **9**, 687–692.
2 R. Humphry-Baker, M. K. Nazeeruddin, J. Burschka, P. Gao, N. Pellet, M. Grätzel and S.-J. Moon, *Nature*, 2013, **499**, 316–319.
3 M. A. Green, A. Ho-Baillie and H. J. Snaith, *Nat. Photonics*, 2014, **8**, 506–514.
4 N. J. Jeon, J. H. Noh, W. S. Yang, Y. C. Kim, S. Ryu, J. Seo and S. Il Seok, *Nature*, 2015, **517**, 476–480.
5 G. Xing, N. Mathews, S. S. Lim, N. Yantara, X. Liu, D. Sabba, M. Grätzel, S. Mhaisalkar and T. C. Sum, *Nat. Mater.*, 2014, **13**, 476–480.
6 W. Hu, R. Wu, S. Yang, P. Fan, J. Yang and A. Pan, *J. Phys. D. Appl. Phys.*, 2017, **50**, 375101.
7 Q. Lin, A. Armin, R. C. R. Nagiri, P. L. Burn and P. Meredith, *Nat. Photonics*, 2014, **9**, 106.
8 E. Edri, S. Kirmayer, S. Mukhopadhyay, K. Gartsman, G. Hodes and D. Cahen, *Nat. Commun.*, 2014, **5**, 3461.
9 J. S. Manser and P. V. Kamat, *Nat. Photonics*, 2014, **8**, 737–743.
10 J. Even, L. Pedesseau, J.-M. M. Jancu and C. Katan, *J. Phys. Chem. Lett.*, 2013, **4**, 2999–3005.
11 M. Maqbool, G. Rehman, L. Ali, M. Shafiq, R. Iqbal, R. Ahmad, T. Khan, S. Jalali-Asadabadi, M. Maqbool and I. Ahmad, *J. Alloys Compd.*, 2017, **705**, 828–839.
12 T. Hakamata, K. Shimamura, F. Shimojo, R. K. Kalia, A. Nakano and P. Vashishta, *Sci. Rep.*, 2016, **6**, 19599.
13 S. D. Stranks and H. J. Snaith, *Nat. Nanotechnol.*, 2015, **10**, 391–402.
14 S. D. Stranks, G. E. Eperon, G. Grancini, C. Menelaou, M. J. P. Alcocer, T. Leijtens, L. M. Herz, A. Petrozza and H. J. Snaith, *Science*, 2013, **342**, 341–344.
15 Z. Shi, S. Li, Y. Li, H. Ji, X. Li, D. Wu, T. Xu, Y. Chen, Y. Tian, Y. Zhang, C. Shan and G. Du, *ACS Nano*, 2018, **12**, 1462–1472.
16 Z. Shi, Y. Li, Y. Zhang, Y. Chen, X. Li, D. Wu, T. Xu, C. Shan and G. Du, *Nano Lett.*, 2017, **17**, 313–321.
17 Z.-F. Shi, Y. Li, S. Li, H.-F. Ji, L.-Z. Lei, D. Wu, T.-T. Xu, J.-M. Xu, Y.-T. Tian and X.-J. Li, *J. Mater. Chem. C*, 2017, **5**, 8699–8706.
18 D. T. Moore, J. M. Luther, T. Chakrabarti, J. A. Christians, A. R. Marshall, E. M. Sanehira, A. Swarnkar and B. D. Chernomordik, *Science*, 2016, **354**, 92–95.
19 M. S. Kirschner, B. T. Diroll, P. Guo, S. M. Harvey, W. Helweh, N. C. Flanders, A. Brumberg, N. E. Watkins, A. A. Leonard, A. M. Evans, M. R. Wasielewski, W. R. Dichtel, X. Zhang, L. X. Chen and R. D. Schaller, *Nat. Commun.*, 2019, **10**, 504.
20 C. Chen, X. Hu, W. Lu, S. Chang, L. Shi, L. Li, H. Zhong and J.-B. Han, *J. Phys. D. Appl. Phys.*, 2018, **51**, 45105.
21 M. Imran, V. Caligiuri, M. Wang, L. Goldoni, M. Prato, R. Krahne, L. De Trizio and L. Manna, *J. Am. Chem. Soc.*, 2018, **140**, 2656–2664.
22 A. Dey, P. Rathod and D. Kabra, *Adv. Opt. Mater.*, 2018, **6**, 1–9.
23 S. Yakunin, M. I. Bodnarchuk, M. V. Kovalenko, A. Walsh, F. Krieg, R. Caputo, C. H. Hendon, L. Protesescu and R. X. Yang, *Nano Lett.*, 2015, **15**, 3692–3696.
24 G. E. Eperon, G. M. Paternò, R. J. Sutton, A. Zampetti, A. A. Haghighirad, F. Cacialli and H. J. Snaith, *J. Mater. Chem. A*, 2015, **3**, 19688–19695.
25 H. Zhou, S. Yuan, X. Wang, T. Xu, X. Wang, H. Li, W. Zheng, P. Fan, Y. Li, L. Sun and A. Pan, *ACS Nano*, 2016, **11**, 1189.
26 V. YP, *Physica*, 1967, **34**, 149.
27 C. Yu, Z. Chen, J. Wang, W. Pfenninger, N. Vockic, J. T. Kenney and K. Shum, *J. Appl. Phys.*, 2011, **110**, 063526.
28 L. Huang and W. R. L. Lambrecht, *Phys. Rev. B: Condens. Matter Mater. Phys.*, 2013, **88**, 165203.
29 A. Shinde, R. Gahlaut and S. Mahamuni, *J. Phys. Chem. C*, 2017, **121**, 14872–14878.
30 S. Hirotsu, *J. Phys. Soc. Japan*, 1971, **31**, 552–560.
31 M. I. Cohen, K. F. Young, T. T. Chang and W. S. Brower, *J. Appl. Phys.*, 1971, **42**, 5267–5272.
32 J. A. Cape, R. L. White and R. S. Feigelson, *J. Appl. Phys.*, 1969, **40**, 5001–5005.
33 M. Hidaka, Y. Okamoto and Y. Zikumaru, *Phys. Status Solidi*, 1983, **263**, 263–269.
34 C. Carabatos-Nédelec, M. Oussaïd and K. Nitsch, *J. Raman Spectrosc.*, 2003, **34**, 388–393.
35 B. T. Diroll, H. Zhou and R. D. Schaller, *Adv. Funct. Mater.*, 2018, **28**, 1800945.
36 S. Rudin, T. L. Reinecke and B. Segall, *Phys. Rev. B: Condens. Matter Mater. Phys.*, 1990, **42**, 11218–11231.
37 A. D. Wright, C. Verdi, R. L. Milot, G. E. Eperon, M. A. Pérez-Osorio, H. J. Snaith, F. Giustino, M. B. Johnston and L. M. Herz, *Nat. Commun.*, 2016, **7**, 11755.
38 R. Saran, A. Heuer-Jungemann, A. G. Kanaras and R. J. Curry, *Adv. Opt. Mater.*, 2017, **5**, 1–9.

